The Lagrangian nature of fingering convection: Supplementary figures

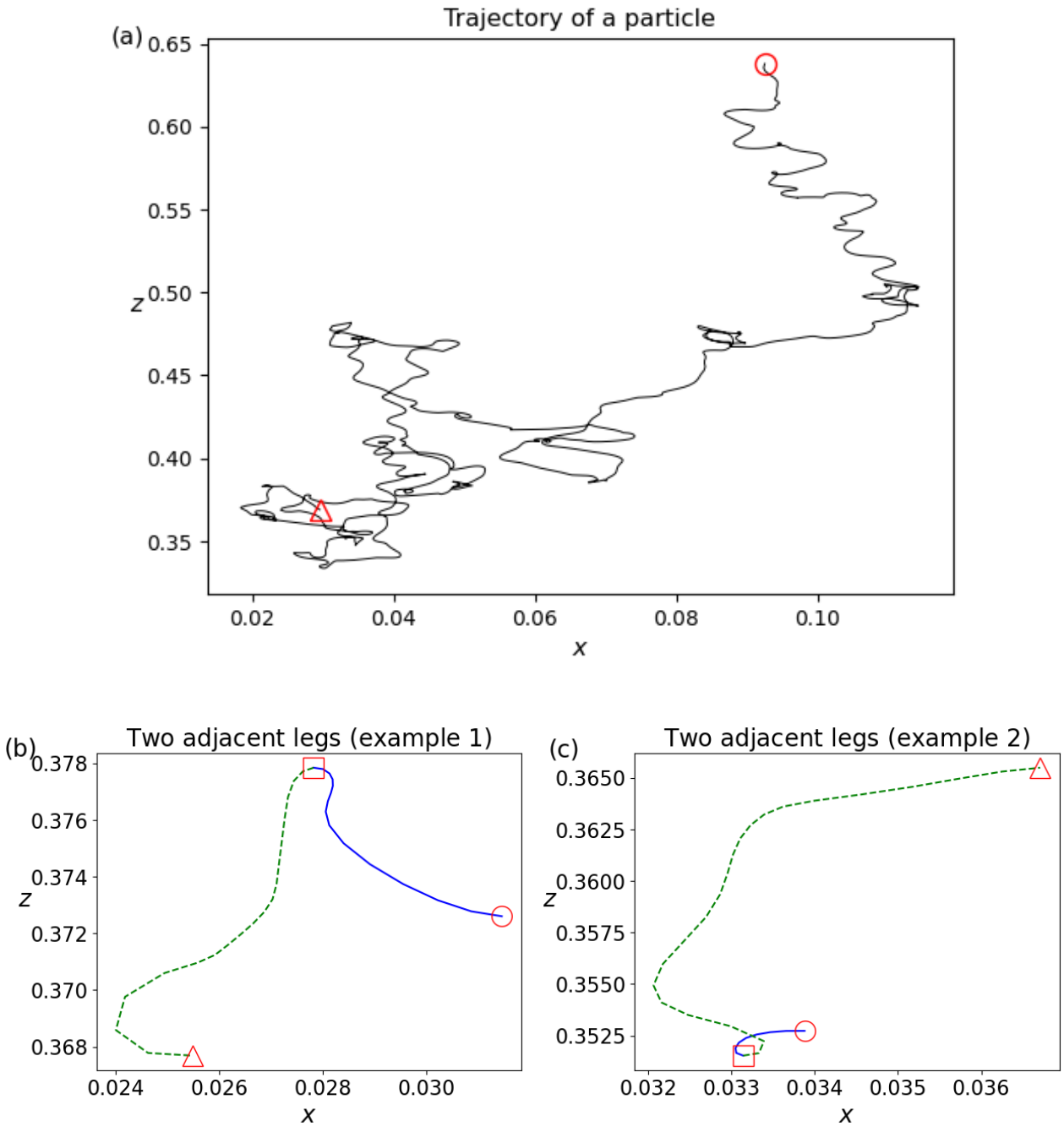

Figure S1: Trajectory of a sample particle and four of its legs (from the simulation with $R_S = 3.16 \times 10^{13}$). The start and end points of each path are marked by circles and triangles, respectively: (*a*) Full trajectory of the sample particle. (*b, c*) Two pairs of adjacent legs singled out from the trajectory displayed in (*a*) with the joint of each pair marked by square. The first leg (solid line) in (b) is of signed length +0.0055 and the second leg (dashed line) is of signed length −0.01; the first leg (solid line) in (c) is of signed length −0.0008 and the second leg (dashed line) is of signed length +0.014.

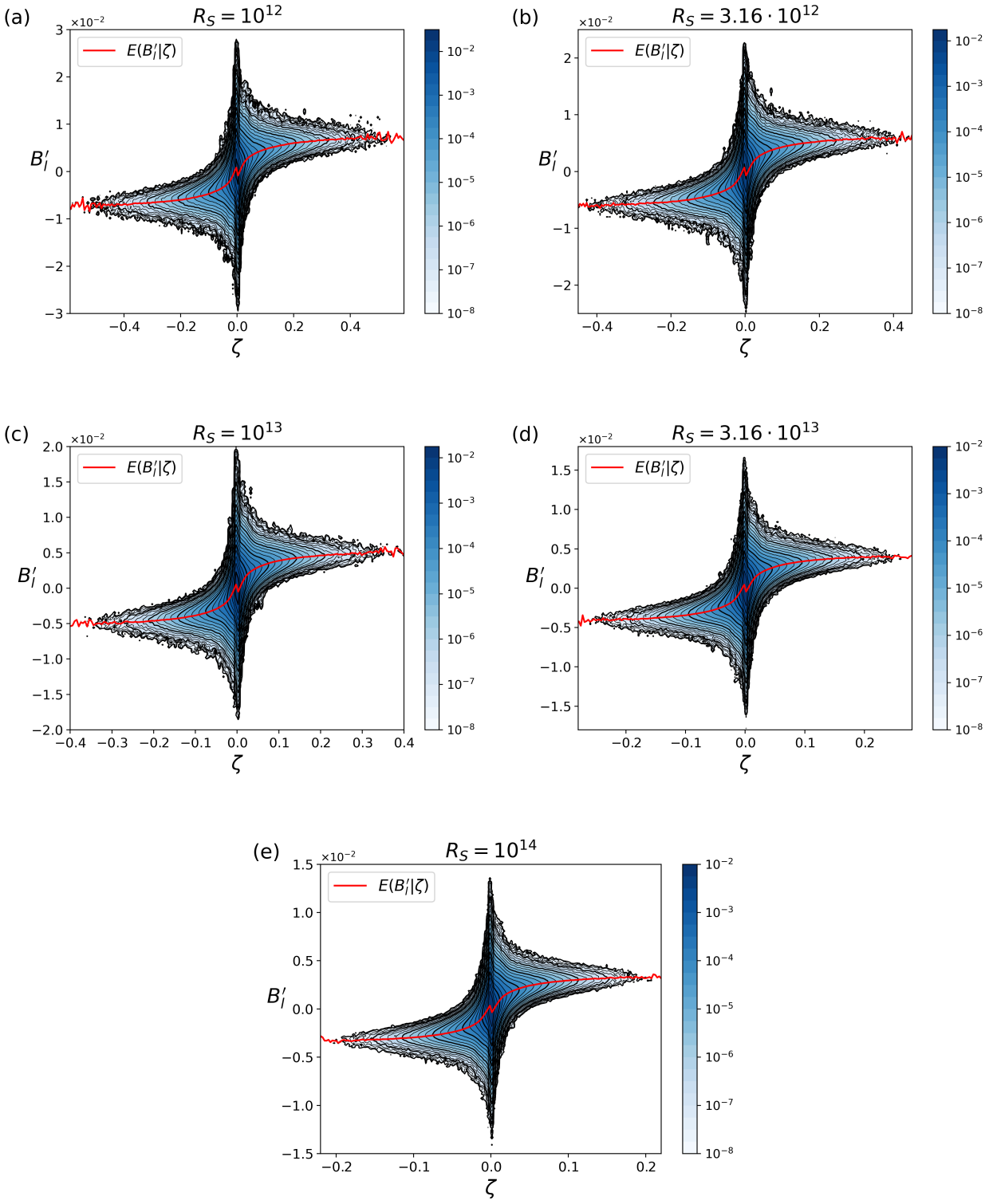

Figure S2: Bivariate frequency (normalized w.r.t. the number of legs, see table 2 in the paper) of leg buoyancy anomaly (B_l') and leg length (ζ) for (a) $R_S = 10^{12}$, (b) $R_S = 3.16 \times 10^{12}$, ($c$) $R_S = 10^{13}$, (d) $R_S = 3.16 \times 10^{13}$, ($b$) $R_S = 10^{14}$. The red curve shows the conditional expectation $E(B_l'|\zeta)$.

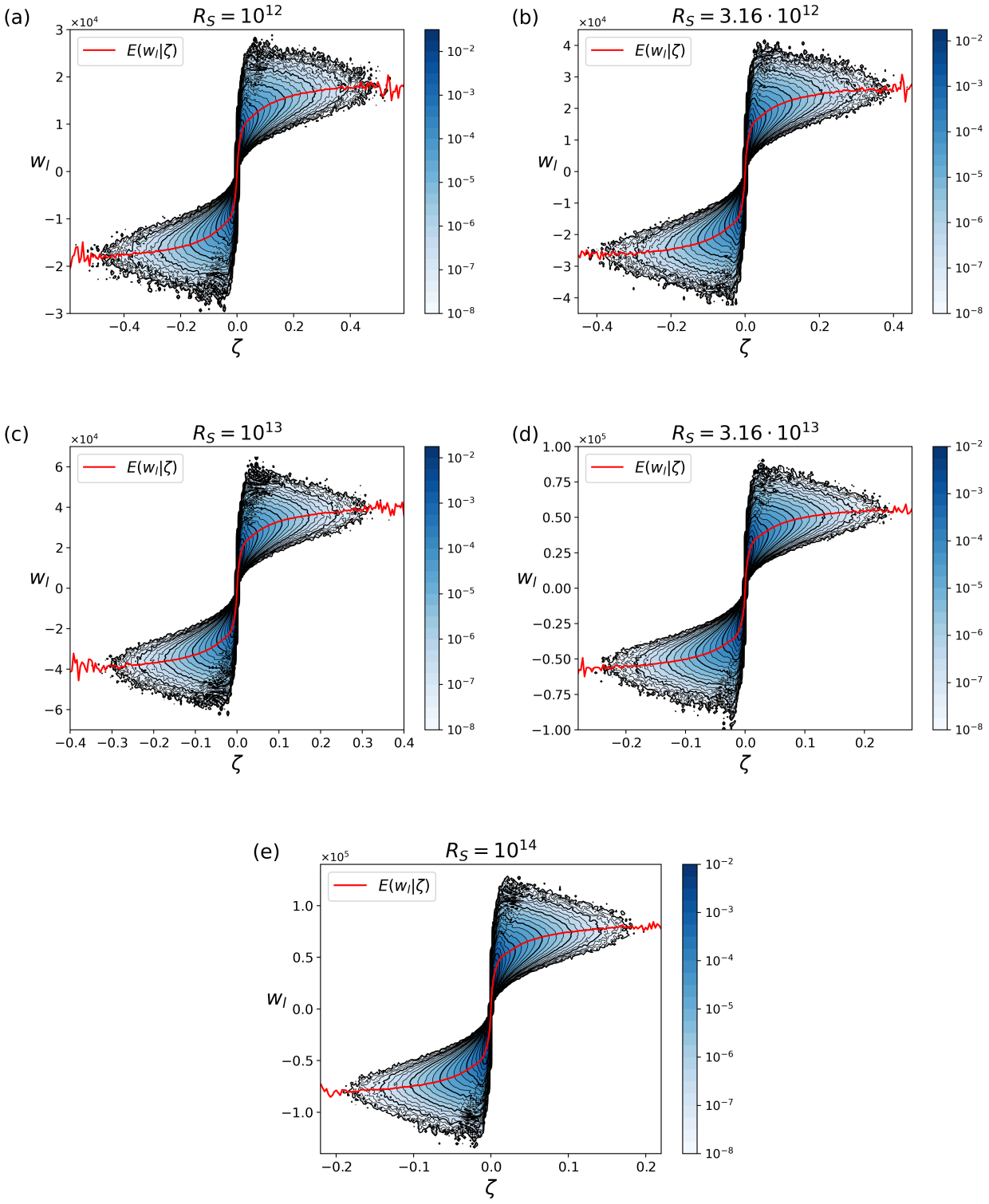

Figure S3: Bivariate frequency (normalized w.r.t. the number of legs, see table 2 in the paper) of leg vertical velocity (w_l) and leg length (ζ) for (a) $R_S = 10^{12}$, (b) $R_S = 3.16 \times 10^{12}$, ($c$) $R_S = 10^{13}$, (d) $R_S = 3.16 \times 10^{13}$, ($b$) $R_S = 10^{14}$. The red curve shows the conditional expectation $E(w_l|\zeta)$.

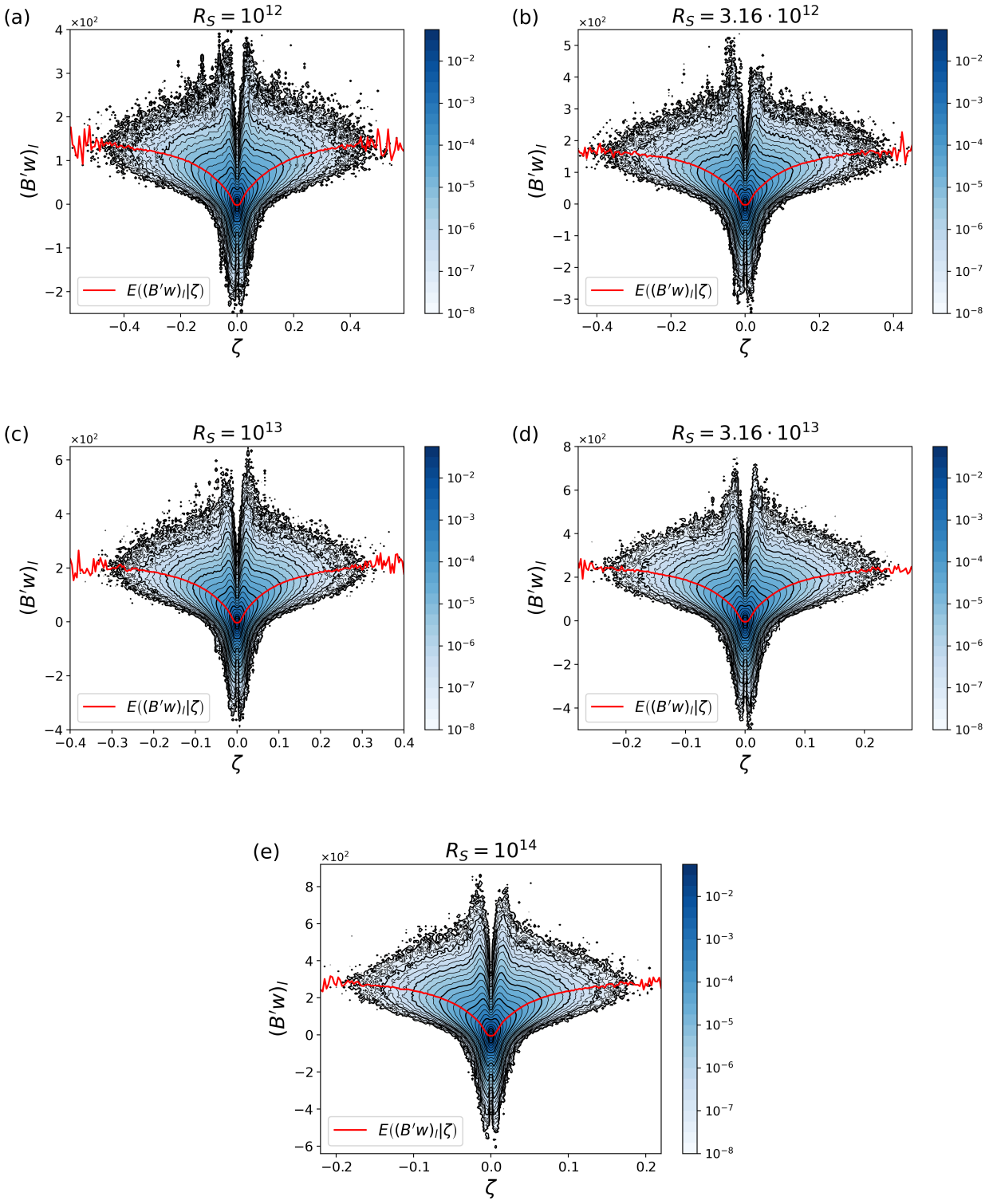

Figure S4: Bivariate frequency (normalized w.r.t. the number of legs, see table 2 in the paper) of leg advective flux ($(B'w)_l$) and leg length (ζ) for (a) $R_S = 10^{12}$, (b) $R_S = 3.16 \times 10^{12}$, ($c$) $R_S = 10^{13}$, (d) $R_S = 3.16 \times 10^{13}$, ($b$) $R_S = 10^{14}$. The red curve shows the conditional expectation $E\left((B'w)_l|\zeta\right)$.

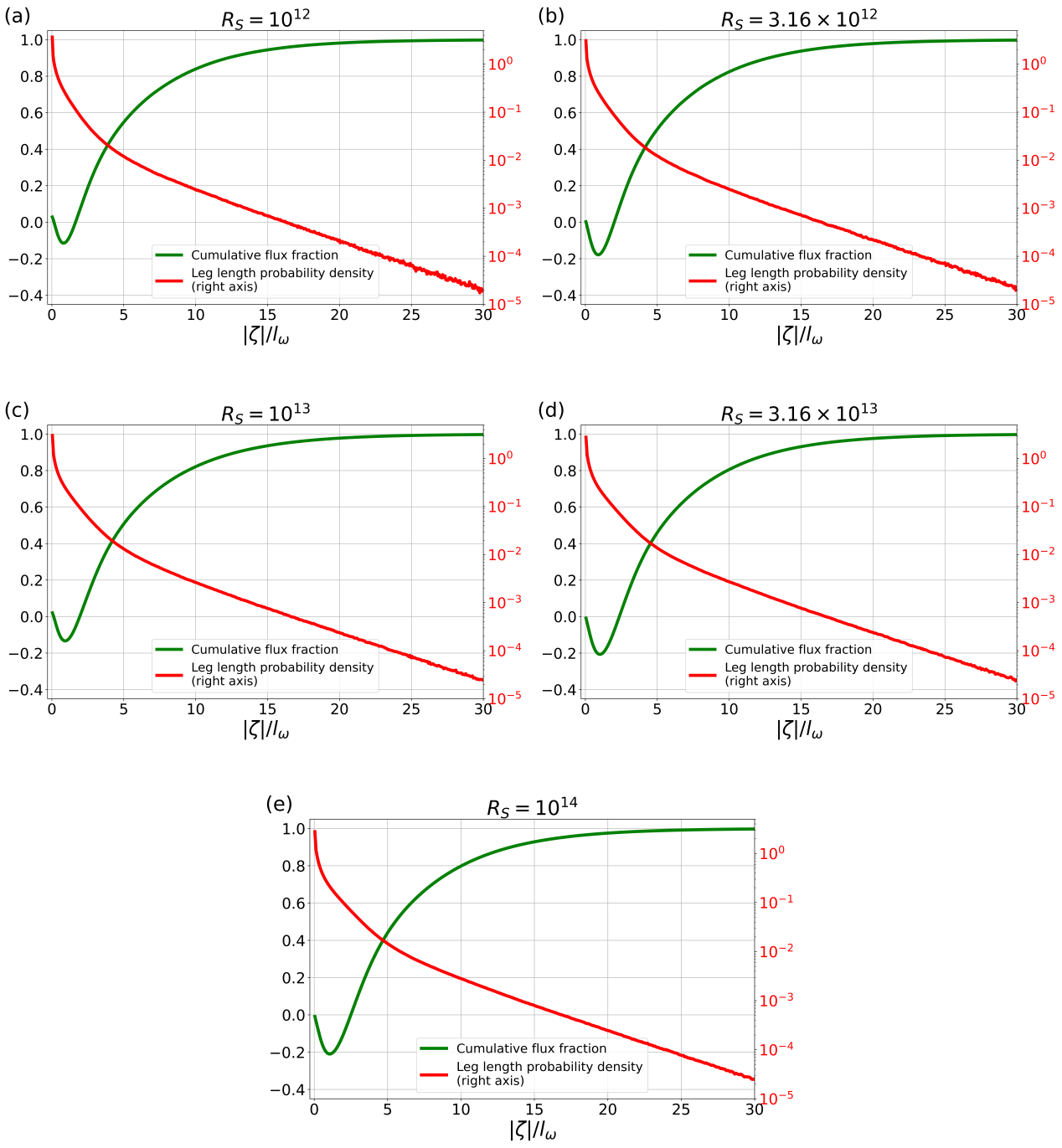

Figure S5: Cumulative flux fraction (green line) as a function of the leg length (left axis). Probability density function of the leg length (red line, right axis, log scale). Panels (a), (b), (c), (d), (e) refer, respectively, to the simulation with $R_S = 10^{12}$, $R_S = 3.16 \times 10^{12}$, $R_S = 10^{13}$, $R_S = 3.16 \times 10^{13}$, $R_S = 10^{14}$.

Figure S6: Online Movie 1: Animation of the ± 0.0035 buoyancy anomaly contours (blue: negative, red: positive) in the central part of the domain of the simulation with $R_S = 10^{14}$. The green dots are the Lagrangian particles. For clarity, only an extremely small fraction of the total number of particles is shown.

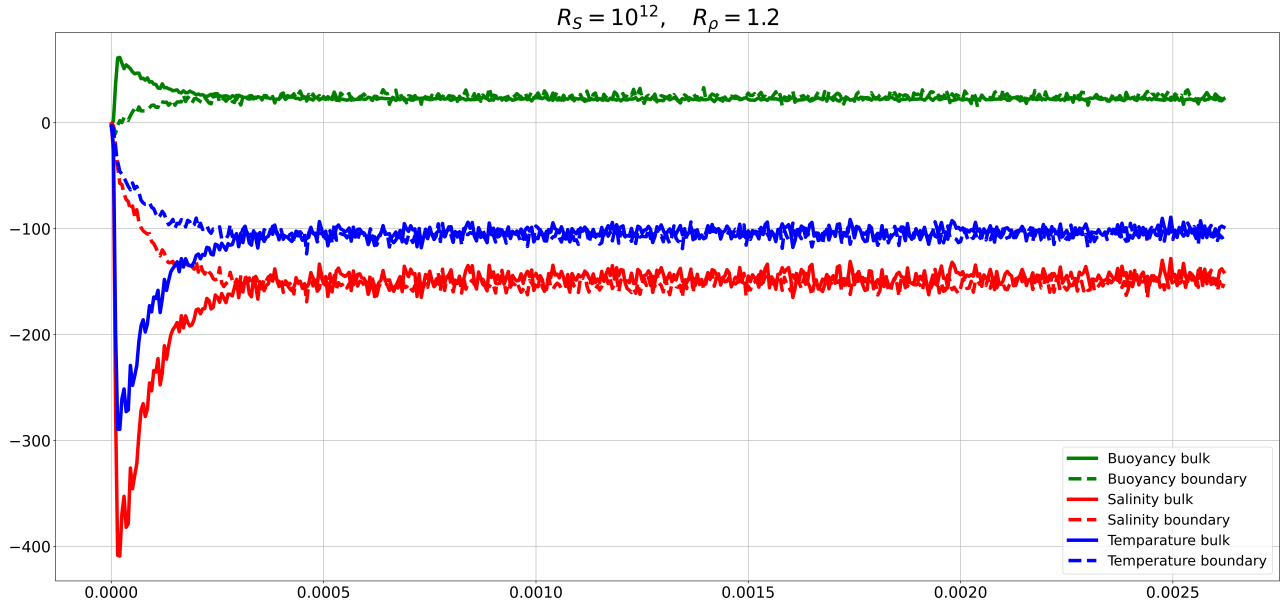

Figure S7: Equilibration of the total temperature, salinity and buoyancy fluxes computed in the bulk of the domain (solid lines), and of the diffusive fluxes of the same quantities computed at the bottom boundary.

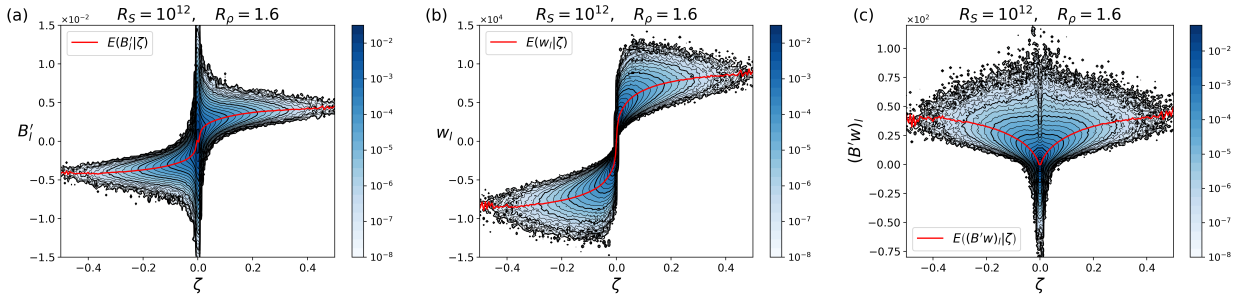

Figure S8: Bivariate frequency (normalized w.r.t. the number of legs, see table 3 in the main text) of (*a*) leg buoyancy anomaly (B_l'), (*b*) leg vertical velocity (w_l), (*c*) leg advective flux ($(B'w)_l$) and leg length (ζ) for $R_S = 10^{12}$, $R_\rho = 1.6$. The red curve shows the conditional expectations $E(B_l'|\zeta)$, $E(w_l|\zeta)$, $E\left((B'w)_l|\zeta\right)$.

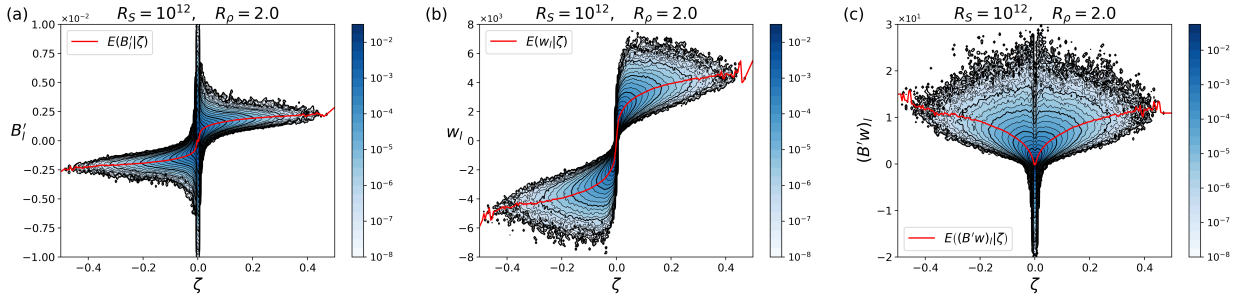

Figure S9: As in Figure S8, but for $R_S = 10^{12}$, $R_\rho = 2.0$.

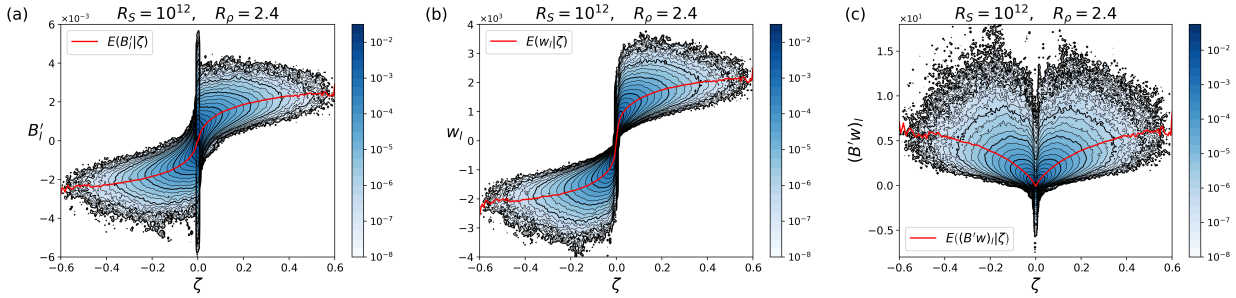

Figure S10: As in Figure S8, but for $R_S = 10^{12}$, $R_\rho = 2.4$.

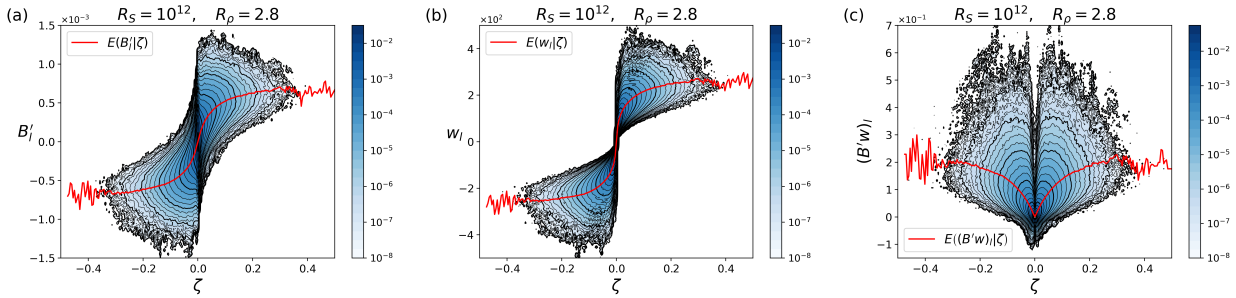

Figure S11: As in Figure S8, but for $R_S = 10^{12}$, $R_\rho = 2.8$.